

New Constraints on Millicharged Particles from Cosmic-ray Production

Ryan Plestid,^{1, 2, 3, 4,*} Volodymyr Takhistov,^{5, †} Yu-Dai Tsai,^{2, 6, ‡}

Torsten Bringmann,^{7, §} Alexander Kusenko,^{5, 8, ¶} and Maxim Pospelov^{9, 10, **}

¹*Department of Physics and Astronomy, University of Kentucky Lexington, KY 40506, USA*

²*Theoretical Physics Department, Fermilab, Batavia, IL 60510, USA*

³*Perimeter Institute for Theoretical Physics, 31 Caroline St. N., Waterloo, Ontario N2L 2Y5, Canada*

⁴*Department of Physics & Astronomy, McMaster University, 1280 Main St. W., Hamilton, Ontario L8S 4M1, Canada*

⁵*Department of Physics and Astronomy, University of California, Los Angeles
Los Angeles, California, 90095-1547, USA*

⁶*Cosmic Physics Center, Fermi National Accelerator Laboratory, Batavia, IL 60510, USA*

⁷*Department of Physics, University of Oslo, Box 1048, N-0371 Oslo, Norway*

⁸*Kavli Institute for the Physics and Mathematics of the Universe (WPI), UTIAS
The University of Tokyo, Kashiwa, Chiba 277-8583, Japan*

⁹*School of Physics and Astronomy, University of Minnesota, Minneapolis, MN 55455, USA*

¹⁰*William I. Fine Theoretical Physics Institute, School of Physics and Astronomy,*

University of Minnesota, Minneapolis, MN 55455, USA

(Dated: March 19, 2022)

We study the production of exotic millicharged particles (MCPs) from cosmic ray-atmosphere collisions, which constitutes a permanent MCP production source for all terrestrial experiments. Our calculation of the MCP flux can be used to reinterpret existing limits from experiments such as MACRO and Majorana on an ambient flux of ionizing particles. Large-scale underground neutrino detectors are particularly favorable targets for the resulting MCPs. Using available data from the Super-K experiment, we set new limits on MCPs, which are the best in sensitivity reach for the mass range $0.1 \lesssim m_\chi \lesssim 0.5$ GeV, and which are competitive with accelerator-based searches for masses up to 1.5 GeV. Applying these constraints to models where a sub-dominant component of dark matter (DM) is fractionally charged allows us to probe parts of the parameter space that are challenging for conventional direct-detection DM experiments, independently of any assumptions about the DM abundance. These results can be further improved with the next generation of large-scale neutrino detectors.

I. INTRODUCTION

The remarkable success of the Standard Model (SM), along with null results for new physics at the LHC, strongly suggests that if new physics exists below the TeV scale it can only be weakly coupled to SM degrees of freedom. While nearly decoupled from the SM, such a *dark sector* would likely leave its strongest imprint on SM degrees of freedom commensurate with its own dynamical energy scales [1]. It is interesting to note that the MeV - GeV regime both contains many SM particles (e.g. muons, mesons, and nucleons) and hosts a number of persistent anomalies, including the anomalous magnetic moment of the muon [2–4]. Furthermore, this energy range is interesting from a phenomenological point of view as it allows for many novel and complementary search strategies that can be used to probe the dark sector. For instance, new physics can often be efficiently probed by fixed target experiments [5–9] with high intensity electron [10, 11] and proton beams [12–20] where dark sector

particles can be produced either directly, or through decays of copious amounts of mesons; collider experiments are also useful probes, especially for higher mass particles with larger couplings where they typically provide the leading constraints [21–23]. A less explored opportunity of discovering dark-sector particles is to consider their production in cosmic-ray interactions, and subsequent detection in large detectors (see e.g. Ref. [24–30]).

Historically, the discovery of SM particles in the MeV-GeV regime (e.g. pions [31] and muons [32]) has harnessed cosmic rays (a proton beam) bombarding the upper atmosphere (a fixed target). The advantage of cosmic rays over accelerator-based fixed target experiments is that the “beam” is always on, there are almost no angular losses (as long as attenuation in rock and atmosphere can be neglected) because the cosmic-ray flux is isotropic, and the detectors located “downstream” can have significant size (e.g. IceCube [33], Super-Kamiokande [34], Hyper-Kamiokande [35], JUNO [36], DUNE [37]). This suggests that cosmic rays, coupled with neutrino telescopes serving as downstream detectors, are a powerful tool with which to probe the dark sector.

In this work, we calculate the flux of millicharged particles¹ (MCPs, see e.g. Ref. [40–44]), χ , arising from meson

* rpl225@uky.edu

† vtakhist@physics.ucla.edu

‡ ytsai@fnal.gov

§ torsten.bringmann@fys.uio.no

¶ kusenko@ucla.edu

** mpospelov@perimeterinstitute.ca

¹ Also known as charged massive particles (CHAMPs) [38, 39].

decays in the upper atmosphere for m_χ in the few MeV to few GeV regime. For this, we adopt a *minimal* MCP model that is based on only two assumptions:

1. The new particle χ couples to the SM photon with a strength $Q_\chi = \epsilon \times e$; we remain agnostic as to the origin of this charge.
2. The new particle is *stable*; this is a natural consequence if Q_χ is the smallest (non-zero) charge in the dark sector.

As these features are relatively generic, MCPs can be thought of as a useful representative example of a stable dark sector particle with which to benchmark the impact of neutrino telescopes. In particular, since we consider only primary production in what follows, our constraints apply (possibly conservatively) to *any* model that satisfies the above two assumptions.

In addition to being a useful benchmark model, MCPs are of interest because of their potential impact on 21cm cosmology (potentially explaining the EDGES anomaly [45–48]), and their natural appearance in models of light dark matter (DM) interacting with the SM via a massless dark photon [49–52]. Boosted millicharged DM can also potentially explain a reported excess in direct detection experiments [53, 54]. Running parallel to these more cosmological motivations, the lack of constraints in the few MeV-few GeV regime has also motivated the proposal of dedicated detectors such as MilliQan [22, 23] and FerMINI [18].

One immediate consequence of our calculation of the cosmic ray-induced MCP flux is that existing bounds on a naturally occurring flux of MCPs can be converted into constraints on Lagrangian parameters ϵ and m_χ , where the MCP charge is $Q_\chi = \epsilon \times e$. In fact, multiple such bounds already exist in the literature, but have never been translated into the $\epsilon - m_\chi$ plane because the relation between ϵ , m_χ and the flux from cosmic rays had never been made explicit. Examples include constraints from MACRO [56, 57], Kamiokande-II [64], LSD [65], CDMS [66] and Majorana [58]. Interestingly we find the resulting constraints to be roughly competitive with those from existing collider experiments, but sub-dominant to reported bounds from neutrino experiments [16, 59, 60].

Here we point out that neutrino telescopes can set new leading bounds on MCP couplings in the 100 MeV–500 MeV regime based on existing data, surpassing the reach of fixed target experiments with neutrino detectors. We demonstrate this point explicitly by providing novel constraints based on published analyses by the Super-Kamiokande (Super-K, SK) collaboration searching for the diffuse supernova neutrino background (DSNB) [55]. Our results, summarized in Fig. 1, suggest that future neutrino telescopes could be able to act as the leading probe of MCPs in this mass regime. Furthermore, our results can be recast as a study of millicharged strongly interacting dark matter (SIDM) [67, 68], allowing us to

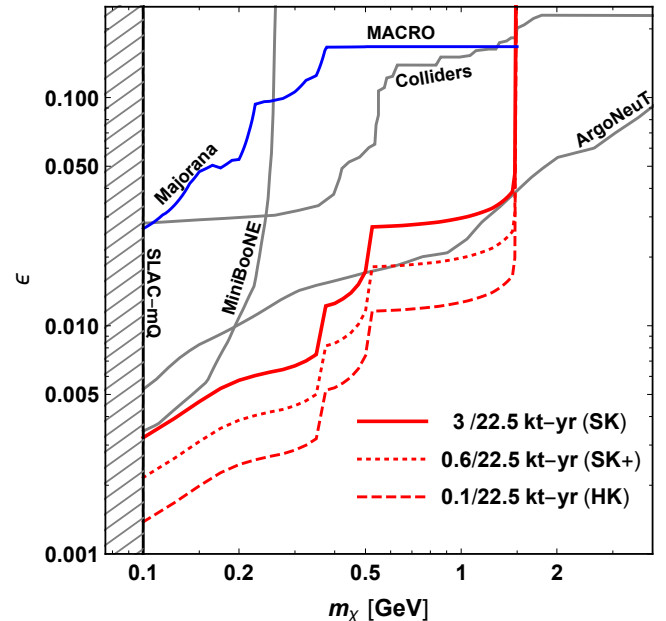


FIG. 1. Exclusion limits for MCPs from cosmic-ray interactions (SK, red solid), obtained using analysis results of the diffuse supernova neutrino background search in Super-K [55], as well as sensitivity projections for an improved SK analysis (SK+, red dotted) and near-future Hyper-K (HK, red dashed). We also display new limits (blue) from recasting data of MACRO [56, 57] and Majorana [58]. Previous limits from fixed target (SLAC MilliQ [10, 11], MiniBooNE [16, 59], ArgoNeuT [60]) and collider experiments [6, 61–63] (as compiled in Ref. [60]) are shown for comparison.

explore a region of interesting parameter space that cannot be easily studied by conventional underground direct-detection experiments (see Section V for a more detailed discussion).

Our study establishes neutrino telescopes as an important probe of the same MCP parameter space that motivated the proposal of MilliQan [22, 23] (and the similarly designed FerMINI [18]), studies on MCP bounds from neutrino experiments [16, 60, 69], and the proposed MCP DM explanation of the EDGES 21 cm anomaly [46, 47, 70]. In the context of MCP DM we emphasize that our constraints are independent of the fractional composition of composition of DM [71–73], for other searches see e.g. Ref. [70, 74–76]. Finally, the explicit calculation of the MCP flux from cosmic rays presented here will enable the use of neutrino telescopes as a robust platform for studying MCPs, free from cosmological assumptions. This has connections to charge quantization, which is itself connected to, but does not necessarily preclude [49], the existence of magnetic monopoles [77], Grand Unification [78–81], and quantum gravity [82].

This paper is organized as follows. In Section II, we discuss the production of mesons from cosmic-ray collisions in the upper atmosphere. In Section III, the MCP

flux from meson decays is calculated. We then discuss the detection of MCPs in neutrino telescopes in Section IV, and outline the kinematics of detecting MCPs. In Section V, we discuss the millicharged SIDM and the constraints and projections that we can place based on our analysis.

II. COSMIC-RAY MESON PRODUCTION

Cosmic rays produce a sizeable number of mesons from interactions in the upper atmosphere, whose subsequent decay produces a continuous flux of MCPs. While the problem can be studied numerically with Monte Carlo simulations, we present here a semi-analytic treatment, allowing us to transparently illustrate the role of key ingredients. Incoming cosmic rays are isotropically distributed on the sky, with the associated flux typically quoted in terms of intensity, $[I_{\text{CR}}] = \text{GeV}^{-1}\text{cm}^{-2}\text{s}^{-1}\text{str}^{-1}$ [83]. In our analysis we take this quantity as implemented in DarkSUSY [84], based on Ref. [85], and focus on the dominant component of cosmic rays, free protons. For convenience, we will instead express the intensity in terms of the center-of-mass boost γ_{cm} for CR protons impinging on atmospheric protons at rest and thus introduce $\mathcal{I}_{\text{CR}}(\gamma_{\text{cm}}) = I_{\text{CR}}(E_p) \times dE_p/d\gamma_{\text{cm}}$, where $\gamma_{\text{cm}} = \frac{1}{2}\sqrt{s}/m_p$, s is the Mandelstam variable for the pp collision, and m_p is the proton mass.

Taking into account that all incoming cosmic rays are eventually absorbed by the atmosphere, the amount of *primary* mesons \mathfrak{m} produced in these collisions is approximately determined by the ratio of the inclusive cross section $\sigma_{\mathfrak{m}}$ for $pp \rightarrow \mathfrak{m}X$ with other particles X to the total inelastic cross section for protons passing through atmospheric matter. We note that this is a rather conservative estimate for the *total* production of mesons given that all final states in these primary interactions tend to trigger further cascades when interacting with the atmosphere, resulting, among others, in a large multiplicity of (lower-energy) meson states. Here we neglect these contributions, which could be studied with a dedicated Monte Carlo simulations of air showers. We model all interactions in the upper atmosphere as pp collisions and therefore take the elastic cross section to be $\sigma_{\text{in}}(pp)$, whose dependence on γ_{cm} is given in Ref. [83]. The resulting meson flux from cosmic-ray collisions in the upper atmosphere is then given by

$$\Phi_{\mathfrak{m}}(\gamma_{\mathfrak{m}}) = \Omega_{\text{eff}} \int \mathcal{I}_{\text{CR}}(\gamma_{\text{cm}}) \frac{\sigma_{\mathfrak{m}}(\gamma_{\text{cm}})}{\sigma_{\text{in}}(\gamma_{\text{cm}})} P(\gamma_{\mathfrak{m}}|\gamma_{\text{cm}}) d\gamma_{\text{cm}}, \quad (1)$$

where $\Omega_{\text{eff}} \approx 2\pi$ is the effective solid angle from which MCPs can arrive at the detector², and $P(\gamma_{\mathfrak{m}}|\gamma_{\text{cm}})$ represents the probability to get a meson with boost $\gamma_{\mathfrak{m}}$ in

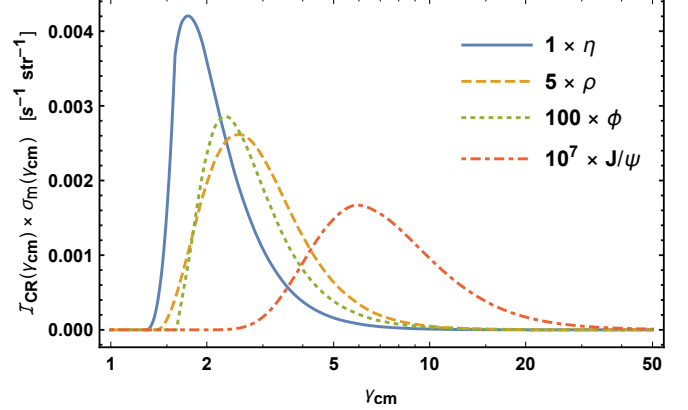


FIG. 2. Differential cosmic-ray intensity multiplied by the meson production cross section as a function of γ_{cm} . For the resulting meson spectra see Fig. 11 in Appendix C.

the lab frame. The latter can be conveniently estimated (see Appendix A 1) from the differential production cross section with respect to $x_F \equiv p_L/p_{\text{max}}$, where p_L is the longitudinal momentum and p_{max} is the maximum possible momentum:

$$P(\gamma_{\mathfrak{m}}|\gamma_{\text{cm}}) \approx \sum_{\alpha} \frac{1}{\sigma_{\mathfrak{m}}} \times \frac{d\sigma_{\mathfrak{m}}}{dx_F} \times \frac{dx_F^{(\alpha)}}{d\gamma_{\mathfrak{m}}}. \quad (2)$$

Here $\alpha = \pm$ denotes the two different possible contributions, see Eq. (A3), and $d\sigma_{\mathfrak{m}}/dx_F$ is a function of γ_{cm} and $x_F(\gamma_{\mathfrak{m}})$.

The meson-production energy spectrum thus depends on both the total meson cross section, $\sigma_{\mathfrak{m}}(\gamma_{\text{cm}})$, and the differential cross section with respect to x_F , or equivalently on $P(\gamma_{\mathfrak{m}}|\gamma_{\text{cm}})$. These quantities must be specified across a significant range of γ_{cm} to reflect the large range of cosmic-ray energies, and we do so by interpolating between existing data for selected values of fixed γ_{cm} (see Appendix B). Although both $\sigma_{\mathfrak{m}}$ and $P(\gamma_{\mathfrak{m}}|\gamma_{\text{cm}})$ influence the final resulting MCP flux, we find that the production cross section (which is also better measured) has a much stronger effect than the differential distribution.

In principle, all possible mesons originating from pp interactions and leading to MCPs (i.e. those with substantial electromagnetic decay modes: π , η , ω , ρ , J/ψ , Υ etc.) as well as direct production via Drell-Yan should be considered. For light MCPs produced via $\pi^0 \rightarrow \gamma\chi\bar{\chi}$ a combination of SLAC's milliQ experiment [10] and LSND's search for electron-like scattering events [86] already strongly restricts the MCP parameter space [16]. We therefore restrict our discussion to the case of heavier

² By rescaling the muon's stopping power [26, 83], we estimate that the energy loss of MCPs in the Earth's crust (standard rock) is

roughly 50 MeV/km for $\epsilon \sim 10^{-2}$. While for the range of ϵ and energies that we are interested in here MCPs interact too strongly to penetrate the entire Earth, they are not significantly impeded to reach the detector when originating from the upper hemisphere.

MCPs, with $m_\chi > \frac{1}{2}m_\pi$, where pion decay to MCPs is kinematically forbidden.

To keep our discussion of meson production tractable, we focus on the dominant η , light vector, and J/ψ mesons. While we have also quantitatively considered Υ meson as well as direct Drell-Yan production, we found these contributions to be negligibly small (six orders of magnitude smaller than J/ψ) since in addition to smaller cross sections these processes require more energetic cosmic rays (with correspondingly much smaller fluxes).

In Appendix B we analyze and fit the available experimental data for η , ρ , ω , ϕ and J/ψ , finding the total production cross section $\sigma_{pp \rightarrow \eta X}(\gamma_{cm})$ as well as the standard spectrum “shape parameterization” $d\sigma_m/dx_F$. In Fig. 2 we display the resulting differential cosmic ray intensity $I_{CR}(\gamma_{cm})$ multiplied by $\sigma_m(\gamma_{cm})$. The shape of these curves is determined by the competition between a rising inclusive cross section and a sharply falling cosmic-ray flux, and illustrates which parts of the cosmic ray spectrum predominantly contributes to a given meson species.

III. MCP FLUX FROM MESON DECAYS

Upon constructing Φ_m as outlined above, we can find the associated flux of MCPs from meson decays by folding the meson flux with the unit-normalized spectrum of MCPs in the lab frame, $P(\gamma_\chi|\gamma_m)$, and weighting by the decay branching ratio

$$\Phi_\chi(\gamma_\chi) = 2 \sum_m \text{BR}(m \rightarrow \chi\bar{\chi}) \int d\gamma_m \Phi_m(\gamma_m) P(\gamma_\chi|\gamma_m), \quad (3)$$

where the factor of 2 accounts for the contribution from both $\bar{\chi}$ and χ . The quantity $P(\gamma_\chi|\gamma_m)$ can be calculated from first principles, at leading order in ϵ , as

$$P(\gamma_\chi|\gamma_m) = \left[\frac{1}{\Gamma} \frac{d\Gamma}{d\gamma_\chi} \right]_{\text{lab}}, \quad (4)$$

where Γ is the decay rate for $m \rightarrow \chi\bar{\chi}$ and $d\Gamma/d\gamma_\chi$ is the differential rate with respect to the MCP boost, both evaluated in the lab frame (see Appendix A 2).

Anticipating MCP detection, we define the integrated “fast-flux” of MCPs satisfying $\gamma_\chi \geq \gamma_{\text{cut}}$ as

$$\Phi_{\text{cut}}(m_\chi, \gamma_{\text{cut}}) = \int_{\gamma_{\text{cut}}}^{\infty} d\gamma_\chi \frac{d\Phi_\chi}{d\gamma_\chi}, \quad (5)$$

where γ_{cut} is set by the relevant experimental threshold. In Fig. 3 we display the mass-dependence of this quantity for several choices of γ_{cut} . The choice $\gamma_{\text{cut}} = 1$ corresponds to the full integrated MCP flux, as relevant for low-threshold ionization experiments, while $\gamma_{\text{cut}} = 6$ is adequate for experiments with an electron recoil threshold of $T_{\min} = 16$ MeV (as relevant for the physics analysis of Super-K discussed below).

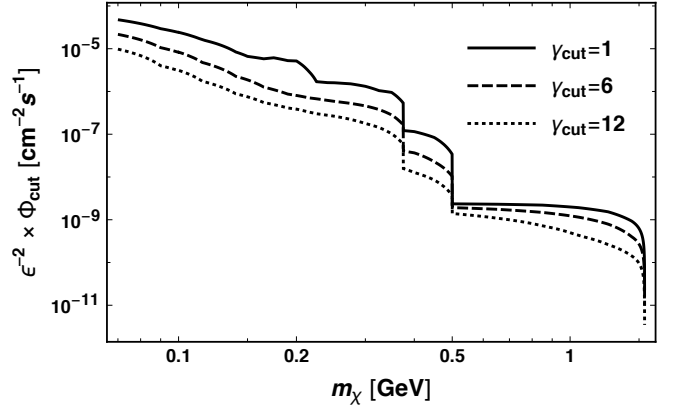


FIG. 3. Fast-flux of MCPs Φ_{cut} due to meson decays as a function of MCP mass, m_χ , for three different choices of γ_{cut} . The spectrum for $\gamma_{\text{cut}} = 1$ is the full integrated MCP flux. The meson mass thresholds are clearly visible, stemming from η , ω/ρ , ϕ , and finally J/ψ (sequentially from left to right).

IV. DETECTING MCPs IN LABORATORIES

As alluded to in the introduction, MCPs can deposit ionization energy directly within detectors, which can be used as a probe of MCP couplings [56–58, 64–66]. Lacking an explicit calculation of cosmic rays as MCP source, previous searches have avoided discussing the mass of the incident MCPs, and instead presented constraints on an ambient MCP flux as a function of the fractional charge ϵ . Our study allows us to directly translate these results (and future searches) into limits on ϵ as a function of m_χ , thus making direct contact with Lagrangian parameters. We discuss the details of this translation in Appendix C 2, and show our results in Fig. 1. We find that ionization experiments are competitive with constraints from colliders around the 100 MeV regime, but quickly become subdominant as m_χ is increased. Significant improvement in detector exposure for ionization searches is expected in future experiments, and our results establish a quantitative baseline that can be used to estimate the potential future impact of upcoming projects such as LEGEND [87]. We note that for MCPs with large charges of $\epsilon \gtrsim 10^{-1}$, as relevant for ionization searches, effects of attenuation when passing through Earth to reach typical detector depths of ~ 1 km of standard rock (i.e. few km water-equivalent) become significant (see e.g. Ref. [26]). Since we do not attempt a detailed translation of ionization bounds in this work, and this region is already well constrained by collider searches (which are not sensitive to attenuation), we do not consider these effects here.

Electron scattering inside Cherenkov detectors, with recoils in the 10 MeV range, is a powerful probe of MCPs [15] (see also [26]). Counting electron-like events with recoil energies, $T'_e = 2m_e(E_e - m_e)$, between T_{\min} and T_{\max} naturally introduces a windowed cross-section

Eq. (C1) which can be well approximated (see Fig. 9) as

$$\tilde{\sigma}_{e\chi}(\gamma_\chi) \approx \frac{2\pi\alpha^2\epsilon^2}{2T_{\min}m_e} \left(1 - \frac{T_{\min}}{T_{\max}}\right) \Theta(\gamma_\chi - \gamma_{\text{cut}}). \quad (6)$$

Here, α is the fine-structure constant, Θ is the Heaviside step function and $\gamma_{\text{cut}} \approx 0.6\sqrt{2T_{\min}/m_e} + 0.4\sqrt{2T_{\max}/m_e}$. The total resulting number of $\chi - e$ scattering events $N_{e\chi}$ for a given experiment is

$$\begin{aligned} N_{e\chi} &= N_e \times t \times \int_{\gamma_{\text{cut}}}^{\infty} d\gamma_\chi \tilde{\sigma}_{e\chi}(\gamma_\chi) \frac{d\Phi_\chi}{d\gamma_\chi}(\gamma_\chi) \quad (7) \\ &\approx N_e \times t \times \frac{\pi\alpha^2\epsilon^2}{T_{\min}m_e} \left(1 - \frac{T_{\min}}{T_{\max}}\right) \times \Phi_{\text{cut}}(m_\chi), \end{aligned}$$

where N_e is the number of electrons within the detector's fiducial volume and t is the data collection period.

Using data sample and analysis results from the DSNB search in Super-K [55] we can place stringent new limits on MCPs from cosmic-ray production. This search looked at inverse beta decays $\bar{\nu}_e p \rightarrow ne^+$ with a positron recoil energy $16 \text{ MeV} < T_{e^+} < 88 \text{ MeV}$, corresponding to $\gamma_{\text{cut}} \approx 6$, effectively reducing the background from cosmic ray muon spallation at lower energies (note that Cherenkov detectors do not directly differentiate between electrons and positrons). As detailed in Appendix C 2, the results of the likelihood analysis performed in Ref. [55] (dashed curve in their Fig. 19) can directly be employed to constrain the recoil electron spectrum from MCPs.

We show our resulting bounds on MCPs in Fig. 1. The limits are competitive with accelerator-driven searches across the $0.1 \lesssim m_\chi \lesssim 1.5 \text{ GeV}$ range. In the range $0.1 \lesssim m_\chi \lesssim 0.5$ neutrino telescopes exceed the leading constraints from both MiniBooNE and ArgoNeuT, demonstrating the potential of neutrino telescopes as a “downstream” detector. The results are quoted in terms of events per year per 22.5 kt of water, corresponding to the fiducial volume of Super-K as employed in Ref. [55].

Upcoming large neutrino experiments will be able to further improve on these results. Additional background suppression due to improved neutron tagging will be possible in an upcoming Super-K upgrade with gadolinium doping [88], which we denote as SK+ and assume a reach of ~ 0.6 events/22.5 kt-yr in Fig. 1. With a fiducial volume of 190 kt the near future Hyper-K water Cherenkov experiment [35] can further improve significantly on results of Super-K. In Fig. 1 we indicate this by assuming a year-long exposure and a sensitivity (in terms of SK's fiducial volume) of ~ 0.1 events/22.5 kt-yr.

Other near future experiments with sizable fiducial volumes, such as DUNE (40 kton, liquid argon) [37] and JUNO (20 kton, liquid scintillator) [36], will complement water-based Cherenkov detectors as probes of the DSNB [89], and hence can also serve as probes of atmospherically-produced MCPs. The solar and spallation backgrounds at low energies are expected to be present in DUNE's DSNB search [90], with an expected

resulting energy cut-off of ~ 20 MeV for a search as in SK. Due to favorable detector configuration and application of pulse-shape discrimination techniques JUNO can perform DSNB search over a wider energy range [91], down to ~ 10 MeV, albeit with overall statistics still considerably lower than that of Hyper-K.

V. STRONGLY-INTERACTING DM

A major focus of DM studies is the direct detection of DM particles using terrestrial detectors [95], typically placed underground. However, these searches depend on the local flux of the DM particles of interest that could reach the experiment. It has long been noted that when the DM-SM particle (mostly nuclei and electrons) cross section is large enough, this flux would be significantly attenuated [67, 96]. The class of DM models featuring such large interactions with ordinary matter is often referred to as strongly interacting DM (SIDM³).

In Ref. [68], DM-SM interactions through a dark photon kinetically mixing with $U(1)_Y$ are studied, focusing on the terrestrial effects on direct detection experiments. In this case, DM scattering with electrons becomes more important than scattering with nuclei, so this is what we focus on in the following. Millicharged DM with cross sections larger than a critical value would have its average energy attenuated and be unable to trigger a detectable signature in ground-based direct-detection experiments [68]. Above this critical cross section, there is a window of available parameter space where MCPs could constitute a sub-dominant component of DM ($\lesssim 0.4\%$ to avoid cosmological constraints [71–73, 98]), from hereon referred to as the millicharged SIDM window. New balloon and satellite experiments have been recently proposed [68] to further explore this window, which could accommodate interesting DM models that could potentially explain the EDGES anomaly [45–48, 99].

In this section, we recast our bounds and projections on MCPs to explore this SIDM window. The results in Fig. 4 are shown in terms of a “reference cross section” typically employed for direct detection experiments to compare the sensitivity reaches of different experiments. For millicharged DM, this is given by⁴

$$\bar{\sigma}_{e,\text{ref}} = \frac{16\pi\alpha^2\epsilon^2\mu_{\chi e}^2}{q_{d,\text{ref}}^4}, \quad (8)$$

where $\mu_{\chi e}$ is the reduced mass of the electron and χ and $q_{d,\text{ref}}$ is the typical momentum transfer in $\chi - e$ scattering

³ This is not identical with “self-interacting DM” [97].

⁴ In Ref. [68], the DM millicharge is generated a coupling to a massless dark photon that kinetically mixes with the SM $U(1)_Y$; here we directly consider the DM to have a millicharge under $U(1)_Y$, with minimal theoretical assumptions about the origin of this charge. The reference cross section we consider corresponds to $\alpha_D = \alpha$ and $m'_A \rightarrow 0$ in Eq. (2.6) of Ref. [68].

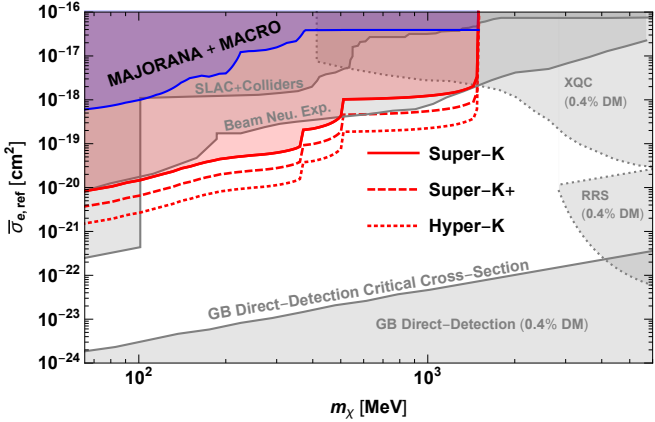


FIG. 4. Constraints and sensitivity reaches that can cover the millicharged SIDM window, including our new bounds from recasting Super-K data [55] (red) and the projection for Super-K (red, dashed) and Hyper-K (red, dotted). We also show the new bounds (blue) from recasting data of MACRO [56, 57] and Majorana [58]. Existing accelerator-based constraints [6, 10, 11, 16, 60–63] and direct-detection limits [68, 92–94] are also shown.

for semiconductor or noble-liquid targets from the local DM flux, taken to be αm_e [68]. Above the “ground-based (GB) direct detection critical cross section”, one can see a regime enclosed by bounds from accelerator-based experiments [6, 10, 11, 16, 60–63], constraints from the above-atmosphere detector (RRS) [92], a rocket experiment (XQC) [93, 94], and underground direct detection experiments [68]. We plot the bound of Super-K and sensitivity reaches for Super-K+, and Hyper-K. We do not consider bounds based on the MCP acceleration from astrophysical sources [26, 38, 39, 100], since they rely on additional assumptions beyond local DM abundance. The constraint on the ultralight dark-photon mediator is also not shown since it is not an essential ingredient for minimal MCPs.

Our results in Fig. 4 establish new constraints on the millicharged SIDM window. It is important to note that our bounds and projections are independent of any assumption about which fraction of the DM is millicharged. Further, for reference cross sections below approximately 10^{-17} cm^2 our results are insensitive to attenuation in the Earth, given that cosmic-ray produced MCPs have much higher energy than that of the local DM flux.

VI. SUMMARY

We have considered MCP production from standard cosmic rays interacting with the atmosphere. This closes a gap in the MCP literature and constitutes a permanent MCP production source for all terrestrial experiments. We presented the first translation of long-standing bounds on an ambient MCP flux into bounds on the MCP charge ϵ as a function of its mass m_χ , and

demonstrated that large-scale underground neutrino experiments are particularly well suited for probing previously inaccessible parameter space. Using existing limits from Super-K’s DSNB search we have placed new limits on MCPs for $0.1 \lesssim m_\chi \lesssim 1.5 \text{ GeV}$, which for $m_\chi \lesssim 0.5 \text{ GeV}$ exceed the sensitivity of fixed target experiments such as MiniBooNE and ArgoNeuT. These new limits are highly relevant also in scenarios where MCPs constitute an SIDM component because they are *i*) independent of the DM fraction made of such MCPs and *ii*) probe a part of the parameter space that cannot be readily tested with conventional direct-detection experiments. The results presented here will be further improved with upcoming large-scale neutrino experiments, and, since we only consider primary meson production, can likely be further strengthened by a more detailed modeling of cosmic-ray showers.

VII. ACKNOWLEDGEMENTS

We would like to thank Dr. T.-T. Yu for a stimulating discussion of the cosmic-ray-generated light dark matter flux. R.P. & Y.-D.T. thank the University of Washington and the Institute for Nuclear theory for its hospitality during the final portion of this work. R.P. also thanks the Fermilab theory group for their hospitality and support. Y.-D.T. would like to thank KICP, University of Chicago, for the hospitality and support. A.K. and V.T. were supported by the U.S. Department of Energy (DOE) Grant No. DE-SC0009937. A.K. was also supported by the World Premier International Research Center Initiative (WPI), MEXT Japan. R.P. was supported by the Government of Canada through an NSERC PGS-D award, and by the U.S. Department of Energy, Office of Science, Office of High Energy Physics, under Award Number DE-SC0019095. This manuscript has been authored by Fermi Research Alliance, LLC under Contract No. DE-AC02-07CH11359 with the U.S. Department of Energy, Office of Science, Office of High Energy Physics. This work was partly performed at the Aspen Center for Physics, which is supported by National Science Foundation grant PHY-1607611. Research at the Perimeter Institute is supported in part by the Government of Canada through NSERC and by the Province of Ontario through MEDT.

Appendix A: Cosmic-ray production kinematics

1. Boost of produced mesons

The lab-frame energy of a meson produced in a collision, E_m , can be written as $E_m = \gamma_{\text{cm}} \mathcal{E} + \gamma_{\text{cm}} \beta_{\text{cm}} \mathcal{P}_{\parallel}$, where curly script variables refer to center of mass frame quantities. We can re-write this expression in terms of $x_F = \mathcal{P}_{\parallel}/p_{\text{max}}$ (“Feynman-x”), where $p_{\text{max}} = \frac{1}{2}\sqrt{s}(1 - m_m^2/s)$ is the largest possible longitudinal momentum

allowed by kinematic constraints; x_F therefore varies from -1 (backwards pointing) to $+1$ (forward pointing). Written in terms of x_F our formula is given by $E_m = \gamma_{cm} p_{max} (\mathcal{E}/p_{max} + \beta_{cm} x_F)$, or

$$\gamma_m = \gamma_{cm} \frac{p_{max}}{m_m} \left(\sqrt{x_F^2 + \frac{p_T^2}{p_{max}^2} + \frac{m_m^2}{p_{max}^2}} + \beta_{cm} x_F \right). \quad (A1)$$

Since $p_T = \mathcal{P}_T \ll p_{max}$ we can neglect it in our analysis. Therefore we can obtain $\gamma_m(x_F)$ from

$$\gamma_m \approx \gamma_{cm} \frac{p_{max}}{m_m} \left(\sqrt{x_F^2 + \frac{m_m^2}{p_{max}^2}} + \beta_{cm} x_F \right). \quad (A2)$$

This equation can be inverted to yield two branches $x_F^{(\pm)}(\gamma_m)$

$$x_F^{(\pm)} = -\gamma_{cm} \gamma_m (\beta_{cm} \pm \beta_m) \frac{m_m}{p_{max}} \quad (A3)$$

corresponding to the two solutions of the quadratic equation.

2. Meson decay to millicharged particles

Most of the decay modes we consider involve two-body final states. For example, in the case of the J/ψ the differential decay in the rest frame of the parent meson is mono-energetic $d\Gamma/d\mathcal{E}_\chi \propto \delta(\mathcal{E}_\chi - \frac{1}{2}m_{J/\psi})$ (in this subsection, curly letters refer to meson rest-frame quantities). Upon boosting to the lab frame this becomes a box distribution, $\text{Box}(E_\chi|\gamma_m)$, of width $E_\chi^{(+)} - E_\chi^{(-)}$ and height $1/(E_\chi^{(+)} - E_\chi^{(-)})$, where

$$E_\chi^{(\pm)} = \gamma_{J/\psi} (\mathcal{E}_\chi \pm \beta_{J/\psi} \mathcal{P}_\chi). \quad (A4)$$

Equivalently, in terms of the MCP's lab frame boosts, we have

$$\gamma_\chi^{(\pm)} = \gamma_{J/\psi} \tilde{\gamma}_\chi (1 \pm \beta_{J/\psi} \tilde{\beta}_\chi), \quad (A5)$$

where $\tilde{\gamma}_\chi$ and $\tilde{\beta}_\chi$ are the boost and velocity of the MCP in the meson rest frame. In the case of ρ^0 and ϕ , the dominant decay mode is also a two body final state (e.g. $\rho^0 \rightarrow \chi\bar{\chi}$). For ω the SM branching ratio for $\omega \rightarrow \pi^0 \ell^+ \ell^-$ is roughly ten times larger than $\omega \rightarrow \ell^+ \ell^-$ [83], but this decay mode is only accessible for $m_\chi \leq \frac{1}{2}(m_\omega - m_\pi) \approx 325$ MeV, as opposed to $m_\chi \leq \frac{1}{2}m_\omega \approx 390$ MeV for the direct two body decay. We therefore neglect this decay mode⁵ which will underestimate the MCP flux by a factor of $\sim O(\text{few})$ in the window $275 \text{ MeV} \gtrsim m_\chi \gtrsim 325 \text{ MeV}$, and focus instead on $\omega \rightarrow \chi\bar{\chi}$. The branching ratio for

MCPs can be obtained by a simple re-scaling of the dimuon branching ratio,

$$\text{BR}(\mathfrak{m} \rightarrow \chi\bar{\chi}) = \epsilon^2 \sqrt{\frac{m_m^2 - 4m_\chi^2}{m_m^2 - 4m_\mu^2}} \text{BR}(\mathfrak{m} \rightarrow \mu^+ \mu^-). \quad (A6)$$

where $\text{BR}(\rho^0 \rightarrow \mu^+ \mu^-) = 4.55 \times 10^{-5}$, $\text{BR}(\omega \rightarrow \mu^+ \mu^-) = 7.4 \times 10^{-5}$, and $\text{BR}(\phi \rightarrow \mu^+ \mu^-) = 2.87 \times 10^{-4}$ [83].

For the Dalitz decay $\eta \rightarrow \gamma\chi\bar{\chi}$ the MCPs are *not* mono-energetic in the meson rest frame. Nevertheless, each infinitesimal rest frame energy \mathcal{E}_χ can be treated as described above provided we integrate over all such \mathcal{E}_χ , weighted by the differential decay rate. Therefore, the lab-frame distribution of MCPs from η decay is given by

$$\left[\frac{1}{\Gamma_\eta} \frac{d\Gamma_\eta}{dE_\chi} \right]_{\text{lab}} = \int d\mathcal{E}_\chi \left[\frac{1}{\Gamma_\eta} \frac{d\Gamma_\eta}{d\mathcal{E}_\chi} \right]_{\text{rest}} \times \text{Box}(E_\chi|\gamma_m), \quad (A7)$$

where $\Gamma_\eta = \Gamma(\eta \rightarrow \chi\bar{\chi}\gamma)$. From Eq. (A7) $P(\gamma_\chi|\gamma_m)$ is readily obtained using Eq. (4) and the chain rule. We neglect the η form factor and compute $\frac{1}{\Gamma} [d\Gamma/d\mathcal{E}]$ using the Wess-Zumino $\gamma\gamma P$ vertex, with P as pseudoscalar meson [101, 102].

Appendix B: Atmospheric meson production rate

Our treatment of meson production in the upper atmosphere is data driven and centers mostly around the ratio of $\sigma(pp \rightarrow \mathfrak{m}X)/\sigma_{\text{inel}}(pp)$ which varies as a function of center of mass energy. Although we have tried to inform our fits using data across a wide range of center of mass energies (or equivalently γ_{cm}) there is a limited window of “important” center of mass boosts that is determined by the competition between a rising inclusive cross section and a sharply falling cosmic-ray flux as a function of γ_{cm} (the typical $I_{\text{CR}} \sim E^{-2.7}$ scaling translates to roughly $I_{\text{CR}} \sim \gamma_{cm}^{-4.5}$). This is illustrated in Fig. 2 where we see that the relevant ranges are γ_{cm} between 1.5-5 for η mesons, between 1.5-10 for ρ (and ω) and ϕ , and between 3-25 for J/ψ .

The rest of this section is devoted to our parameterization of the available inclusive cross section data, which we separate into a discussion of $\sigma_m(\gamma_{cm})$ and $P(\gamma_m|\gamma_{cm})$. It is important to note that although $P(\gamma_m|\gamma_{cm})$ is poorly constrained by the data we were able to find, its impact on our sensitivity curves is marginal; this is because the total number of MCPs produced is independent of this quantity. In contrast, although it has a relatively comprehensive dataset, the production cross section $\sigma_m(\gamma_{cm})$ in the window of maximal production (as shown in Fig. 2) can have a substantial impact on the MCP signal (bounds on ϵ scale as $\sqrt[4]{\text{signal}}$) because it alters the total number of MCPs produced. We therefore anticipate that the uncertainties in the production cross section are the dominant source of error in our analysis (at the level of $\sim O(\text{few})$).

⁵ Including $\omega \rightarrow \pi^0 \chi\bar{\chi}$ would involve a chiral perturbation theory calculation analogous to the one performed for $\eta \rightarrow \gamma\chi\bar{\chi}$.

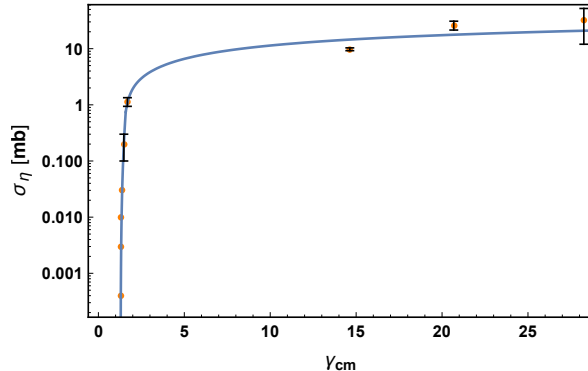


FIG. 5. Production cross section for $pp \rightarrow \eta X$ as a function of $\gamma_{\text{cm}} = \frac{1}{2}\sqrt{s}/m_p$. The data is taken from Refs. [103–108] and fitted using the piece-wise procedure described in the text; the smooth curve is Eq. (B1). .

1. η mesons

Eta meson production in pp collisions has been most extensively measured in the near-threshold regime for the exclusive process $pp \rightarrow \eta pp$ [103, 108]. Near threshold this is the only available channel, such that this cross section can be taken as a reasonable estimate of the total inclusive cross section. Further away from threshold bona fide measurements of the inclusive cross section are scarcer but we have identified four measurements in the literature at $\sqrt{s} = 3.17, 27.45, 38.8$, and 53 GeV [103–107]. We split the available data into two subsets, near-threshold exclusive production (defined as $pp \rightarrow pp\eta$ measurements for $\sqrt{s} \leq 3$ GeV) and far-from-threshold inclusive data (defined as $pp \rightarrow \eta X$ for $\sqrt{s} > 3$ GeV). We fit the near-threshold data for $\sigma_\eta(\sqrt{s})$ with the function $f(x) = a(x - 2.42)^b x^c$ where $x \equiv \sqrt{s_{pp}}/\text{GeV}$. For the far-from-threshold data we instead use $g(x) = a(1 + |b|/(x - 2.42)^2) \log^2(x)$. In both cases a weighted linear regression to the data was performed. Using the best fit values for both fits, and demanding that the function is continuous we find

$$\sigma_\eta(\gamma_{\text{cm}}) = \Theta(\gamma_{\text{cm}} - \gamma') f(1.876\gamma_{\text{cm}}) + \Theta(\gamma' - \gamma_{\text{cm}}) g(1.876\gamma_{\text{cm}}), \quad (\text{B1})$$

where the numerical factor comes from the relationship $\sqrt{s} = 2m_p\gamma_{\text{cm}} = (1.876 \text{ GeV})\gamma_{\text{cm}}$. The functions $f(x)$ and $g(x)$, with their best fit values, are given by

$$f(x) = (0.0176 \text{ mb}) \times (x - 2.42)^{2.22} x^{4.59} \quad (\text{B2})$$

$$g(x) = (1.32 \text{ mb}) \log^2(x) \times \left(1 + \frac{0.356}{(x - 2.42)^2}\right)^{-1}, \quad (\text{B3})$$

and $\gamma' = 1.59$ is chosen such that Eq. (B1) is continuous; the fit is shown vs. the data (with error bars when available) in Fig. 5.

For the differential cross section $d\sigma_m/dx_F$, measurements at NA27 [104] strongly suggest an exponential dis-

tribution,

$$\frac{d\sigma_\eta}{dx_F} = \sigma_\eta \times \frac{c_\eta/2}{1 - \exp[-c_\eta]} \exp\left[-\frac{|x_F|}{c_\eta}\right], \quad (\text{B4})$$

where c_η depends on γ_{cm} . Measurements from NA27 at $\sqrt{s} = 27.5$ GeV (corresponding to $\gamma_{\text{cm}} = 14.6$) fix $c_\eta \approx 9.5$ [104]. One generally expects that c_η will be a monotonically increasing function of γ_{cm} , and that $c_\eta > 0$. The simplest functional form that satisfies these expectations, and agrees with the measurement of [104] is

$$c_\eta(\gamma_{\text{cm}}) = 9.5 + (\text{slope}) \times (\gamma_{\text{cm}} - 14.6); \quad (\text{B5})$$

we take $\text{slope} \approx \frac{1}{2}$. We checked that our sensitivity to MCPs from experiments such as SK are relatively insensitive to the value of the slope parameter.

2. Light vector mesons

The production cross section for the ρ^0 meson is relatively well measured [103, 107, 108]. Like the η meson we perform a best fit analysis with the function $g(x)$, but without weighted errors. We find the data to be reasonably well described by

$$\sigma_\rho(\gamma_{\text{cm}}) \approx (1.35 \text{ mb}) \log^2(1.876\gamma_{\text{cm}}) \times \left(1 + \frac{13.4}{(1.876\gamma_{\text{cm}} - 2.61)^2}\right)^{-1}. \quad (\text{B6})$$

A comparison between the available data and our smooth fit is shown in Fig. 6.

We found that the data for $\sigma(pp \rightarrow \rho X)$ had a much better coverage than the corresponding ω production cross section, and where there are measurements of the ω cross section it is nearly identical to the ρ cross section. We therefore estimated the ω cross section $\sigma_\omega(\gamma_\omega) \simeq \sigma_\rho(\gamma_\rho)$.

For the ϕ meson we find that the functional form $h(x) = a(1 + |b|/(x - 2.896)^2)^{-1} x^c$ gives a reasonable fit to the data [103, 107, 108]. After an unweighted regression we find that σ_ϕ is well described, c.f. Fig. 7, by

$$\sigma_\phi(\gamma_{\text{cm}}) = (0.01 \text{ mb}) (1.876\gamma_{\text{cm}})^{1.23} \times \left(1 + \frac{2.4}{(1.876\gamma_{\text{cm}} - 2.896)^2}\right). \quad (\text{B7})$$

Like the η meson, the longitudinal momentum distributions for the vector mesons were more difficult to find in the literature, and we rely on a single measurement at $\sqrt{s} = 27.5$ GeV [104] which shows the x_F dependence to be described by Eq. (B4) with $c_V = c_\rho = c_\omega = c_\phi \approx 7.7$. We expect this value to be smaller at lower center of mass energies and so take

$$c_V = 7.7 + \frac{5.7}{13}(\gamma_{\text{cm}} - 14.6), \quad (\text{B8})$$

which, just like the c_η , should be viewed as a cartoon of the behaviour of $d\sigma/dx_F$ as a function of γ_{cm} rather than a faithful representation.

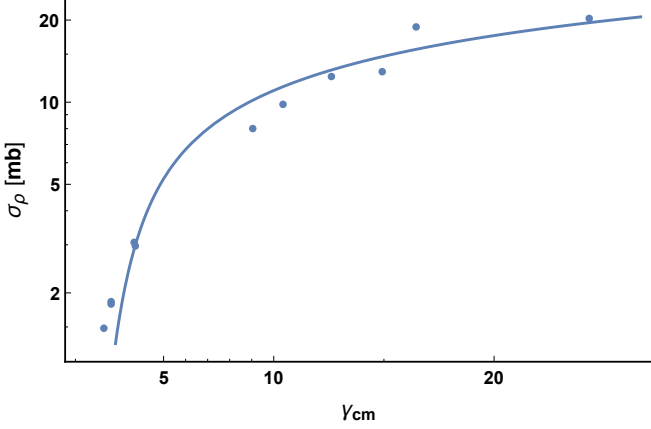


FIG. 6. Compilation of $pp \rightarrow \rho X$ cross sections as a function of γ_{cm} taken from [103, 107, 108].

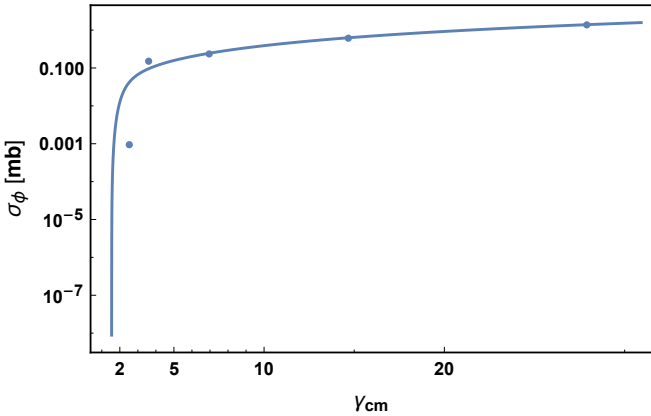


FIG. 7. Compilation of $pp \rightarrow \phi X$ cross sections as a function of γ_{cm} taken from [104, 107, 108].

3. J/ψ mesons

For the J/ψ mesons we found two convenient summaries of the available data: one from E-739 (Fig. 7 in Ref. [109]) and one from HERA-B (Fig. 8 of Ref. [110]). The HERA-B compilation includes measurements at significantly higher center of mass energies. For comparison we plot both sets of data in Fig. 8 where we see that the HERA-B compiled data is roughly consistent with that from the E739 paper, but suggests a steeper growth with rising center of mass energy. We use the best fit to the former to calculate $\sigma_m(\gamma_{\text{cm}})$.

For the differential distribution we used the standard parameterization of $d\sigma_{J/\psi}/dx_F$ [111]

$$\frac{d\sigma_{J/\psi}}{dx_F} = \sigma_{J/\psi} \times \frac{(c_{J/\psi} + 1)}{2} (1 - |x_F|)^{c_{J/\psi}}. \quad (\text{B9})$$

Like c_η , the fit parameter $c_{J/\psi}$ depends on the center of mass energy, and like c_η the precise value of $c_{J/\psi}$ has a relatively mild effect on the fast-flux of MCPs. Data from experiments at lower energies show a preference for

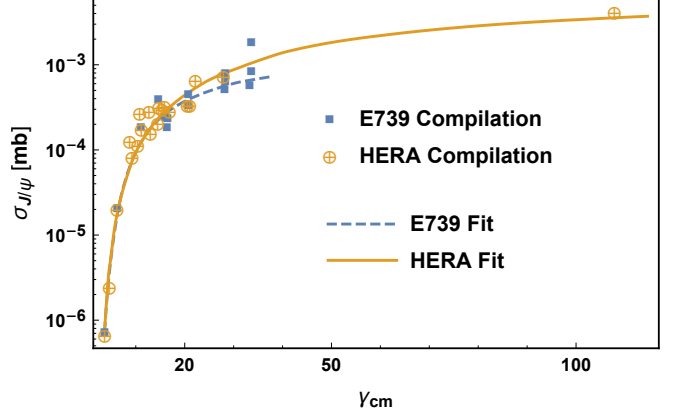


FIG. 8. Production cross section for $pp \rightarrow J/\psi X$ as a function of $\gamma_{\text{cm}} = \frac{1}{2}\sqrt{s}/m_p$. The data points have been digitized from E-789's compilation [109] and HERA-B's compilation [110]. The solid curve is digitized from the fit presented in Ref. [110] while the dashed curve is taken from Ref. [109]. For our sensitivity analysis we use the solid curve from [110].

$c_{J/\psi} \approx 2$ for $\sqrt{s} \leq 15$ GeV [111] whereas experiments at higher energies find larger values such as $c_{J/\psi} \approx 6$ for $\sqrt{s} \approx 40$ GeV [112]; we did not find a robust set of measurements of $c_{J/\psi}$ spanning the entire range of γ_{cm} relevant for cosmic ray pp collisions. For simplicity, and because our final results are relatively insensitive to the details of the x_F distribution, we take $c_{J/\psi}$ to vary linearly with γ_{cm} ,

$$c_{J/\psi} = 2 + \frac{1}{5}(\gamma_{\text{cm}} - 5). \quad (\text{B10})$$

In this case, there is data at lower center of mass energies that suggests this formula is a reasonable interpolation.

Appendix C: MCP signal in experiments

1. MCP-electron scattering

The detection of MCPs is dominated by soft scattering from electrons as can be readily understood by considering the differential scattering cross section which, being mediated by photon exchange, scales as $d\sigma/dQ^2 \sim 1/Q^4$. For elastic scattering from a target of mass M , the momentum transfer is given by $Q^2 = 2M(E' - M)$, where E' is the total recoil energy of the target. The cross section is therefore maximized by scattering off the lightest target possible with the lowest possible recoil energy. In practice, experimental considerations such as detection efficiency and background reduction will set a minimum electron recoil energy which will, in turn, dictate the detection cross section for that given experiment. We will therefore consider a windowed cross section for electron recoils with kinetic energy, $T'_e = (E'_e - m_e)$ between T_{min}

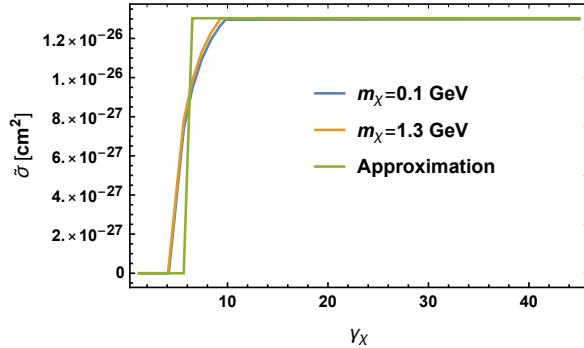


FIG. 9. Dependence of windowed cross section $\tilde{\sigma}_{e\chi}$ on MCP boost factor γ_χ for $T'_{\min} = 16$ MeV and $T'_{\max} = 80$ MeV as compared to the approximation Eq. (6).

and T_{\max} , or equivalently with momentum transfers between Q_{\min}^2 and Q_{\max}^2 ,

$$\tilde{\sigma}_{e\chi} = \int_{Q_{\min}^2}^{Q_{\max}^2} \frac{d\sigma_{e\chi}}{dQ^2} dQ^2. \quad (\text{C1})$$

Since the four-momentum transfer is directly related to the recoil energy in the lab frame, $T'_e = E'_e - m_e$, via $Q^2 = -2(p_e - p'_e)^2 = (2m_e E'_e - 2m_e^2) = 2m_e T'_e$, this is equivalent to demanding that $Q^2 \geq 2m_e T_{\min}$. In the center of mass frame the maximal momentum transfer is given when the scattering is back-to-back such that $Q^2 \leq 4P_e^2 - 2m_e^2$ where P_e is the electron's momentum in the center of mass frame,

$$\mathcal{P}_e = \sqrt{\frac{m_e^4 - 2m_e^2(m_\chi^2 + s) + (m_\chi^2 - s)^2}{4s}} \quad (\text{C2})$$

In terms of lab frame variables this implies that

$$T'_e \leq \frac{2m_e P_\chi^2}{2m_e E_\chi + m_e^2 + m_\chi^2} \approx 2m_e(\beta_\chi \gamma_\chi)^2 \quad (\text{C3})$$

where the approximation holds provided $m_\chi \gg m_e \gamma_\chi$. The main consequence of Eq. (C3) is that the lower bound of integration in Eq. (C1) is given (at leading order in m_e/E_χ)⁶ by $Q_{\min}^2 = \max(2m_e T_{\min}, 4m_e^2(\beta_\chi \gamma_\chi)^2)$, and the upper bound is given by $Q_{\max}^2 = \min(2m_e T_{\max}, 4m_e^2(\beta_\chi \gamma_\chi)^2)$. The effect of this approximation on $\tilde{\sigma}_{e\chi}$ is stated as Eq. (6) in the main text and illustrated in Fig. 9. In summary, the primary driver of the windowed cross section is whether or not the incident MCP is sufficiently boosted to kick the electron above the detection threshold. In principle, the thresholds of large neutrino detectors can be rather low, a few MeV in case of SK, and as low as 200 keV for

Borexino. We choose, however, a much higher threshold of $\sim 15 - 16$ MeV, that removes all the events generated by solar neutrinos, so that background counting rates reduce to $O(\text{few})$ per year.

In the case of $e\chi$ scattering the event shape spectrum is determined by the differential cross section with respect to recoil energy, $d\tilde{\sigma}/dT_e \propto 1/T_e^2$, and the incident flux of MCPs. We have confirmed that this shape is very similar to the case of a neutrino spectrum described by temperature of $T_\nu \lesssim 5$ MeV [55], allowing us to readily employ those results.

We emphasize that the DSNB limits from Super-K are given in terms of limits on the scattered positron event rate as a function of the effective neutrino temperature T_ν from supernova emission. We note, for the reader's convenience, that in [55] there are two bounds quoted: one for an ensemble of supernovae of different temperatures and one for a single supernova temperature. We use the latter, because it more closely mimics our signal as is clearly shown in Fig. 10 (the diffuse ensemble would be relatively flat as a function of energy).

2. Ionization experiments

Ionization is a very low threshold process and so we use the full flux (integrated over all boosts γ_χ) of MCPs for ionization experiments; this corresponds to $\gamma_{\text{cut}} = 1$ as shown in Fig. 3; we denote this total flux by $\Phi(m_\chi)$. To translate existing bounds on an ambient MCP flux in the literature we demand that

$$\epsilon^2 \times (\epsilon^{-2} \Phi(m_\chi)) = \Phi_{\text{ion}}(\epsilon), \quad (\text{C4})$$

where $\epsilon^{-2} \Phi(m_\chi)$ corresponds to the $\gamma_{\text{cut}} = 1$ curve in Fig. 3 (i.e. the integrated MCP flux generated in the upper atmosphere), and $\Phi_{\text{ion}}(\epsilon)$ is the joint exclusion curve obtained by combining data from MACRO [56, 57] and Majorana [58] as shown in Fig. 7 of [58]. We then solve for ϵ for each value of m_χ which determines a critical value of, $\epsilon_c(m_\chi)$, above which MCPs are excluded.

3. Meson fluxes

A useful biproduct of our research are the lab-frame spectra of mesons as a function of γ_m . Given any calculable $m \rightarrow$ dark sector decay, using the meson spectra as inputs, a flux of dark sector particles originating from primary cosmic-ray collisions can be obtained. Our results, shown in Fig. 11, rely only on simple parameterizations of the differential cross sections $d\sigma/dx_F$ and the measured production cross sections as outlined in Appendix B.

⁶ In producing our exclusion curves we use the full expression in Eq. (C3) rather than the indicated approximation.

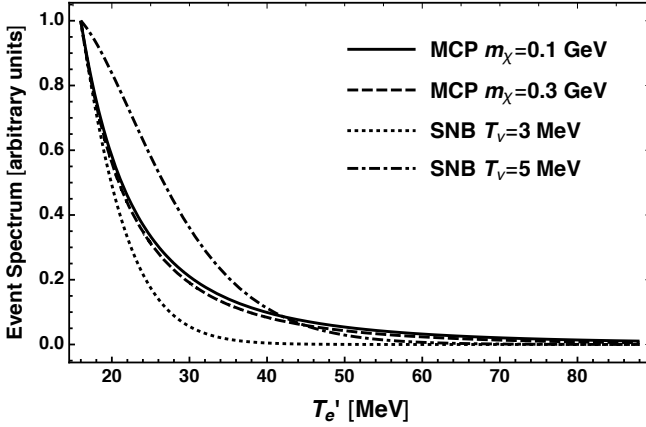


FIG. 10. Comparison of event shapes for MCP elastic scattering off electrons and inverse beta decay from supernova background neutrinos. The MCP signal was obtained by folding the differential scattering cross section $d\sigma_{e\chi}/dT_e$ against the cosmic-ray induced MCP flux. The supernova background curves correspond to $E_\nu^2/(e^{E_\nu/T_\nu} + 1)$ where $E_\nu = T_e + 1.3$ MeV; these correspond to the fixed temperature profiles used in Ref. [55] as can be readily verified by reproducing their Fig. 19.

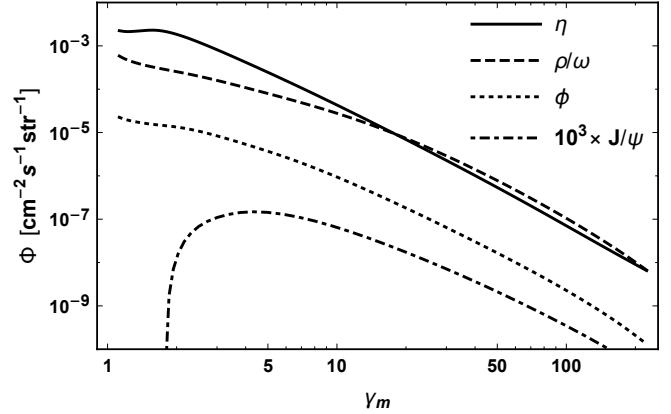


FIG. 11. Mesons fluxes from primary pp collisions assuming a longitudinal momentum distribution as described in Eqs. (B4), (B5) and (B8) to (B10).

[1] Jim Alexander *et al.*, “Dark Sectors 2016 Workshop: Community Report,” (2016) arXiv:1608.08632 [hep-ph].

[2] G. W. Bennett *et al.* (Muon g-2), “Final Report of the Muon E821 Anomalous Magnetic Moment Measurement at BNL,” Phys. Rev. **D73**, 072003 (2006), arXiv:hep-ex/0602035 [hep-ex].

[3] Fred Jegerlehner and Andreas Nyffeler, “The Muon g-2,” Phys. Rept. **477**, 1–110 (2009), arXiv:0902.3360 [hep-ph].

[4] James P. Miller, Eduardo de Rafael, B. Lee Roberts, and Dominik Stöckinger, “Muon (g-2): Experiment and Theory,” Ann. Rev. Nucl. Part. Sci. **62**, 237–264 (2012).

[5] James D. Bjorken, Rouven Essig, Philip Schuster, and Natalia Toro, “New Fixed-Target Experiments to Search for Dark Gauge Forces,” Phys. Rev. **D80**, 075018 (2009), arXiv:0906.0580 [hep-ph].

[6] Rouven Essig *et al.*, “Working Group Report: New Light Weakly Coupled Particles,” in *Proceedings, 2013 Community Summer Study on the Future of U.S. Particle Physics: Snowmass on the Mississippi (CSS2013): Minneapolis, MN, USA, July 29-August 6, 2013* (2013) arXiv:1311.0029 [hep-ph].

[7] Brian Batell, Maxim Pospelov, and Adam Ritz, “Exploring Portals to a Hidden Sector Through Fixed Targets,” Phys. Rev. **D80**, 095024 (2009), arXiv:0906.5614 [hep-ph].

[8] J. P. Lees *et al.* (BaBar), “Search for a Dark Photon in e^+e^- Collisions at BaBar,” Phys. Rev. Lett. **113**, 201801 (2014), arXiv:1406.2980 [hep-ex].

[9] Rouven Essig, Philip Schuster, Natalia Toro, and Bogdan Wojtsekhowski, “An Electron Fixed Target Experiment to Search for a New Vector Boson A’ Decaying to e^+e^- ,” JHEP **02**, 009 (2011), arXiv:1001.2557 [hep-ph].

[10] A. A. Prinz *et al.*, “Search for millicharged particles at SLAC,” Phys. Rev. Lett. **81**, 1175–1178 (1998), arXiv:hep-ex/9804008 [hep-ex].

[11] Alyssa Ann Prinz, *The Search for millicharged particles at SLAC*, Ph.D. thesis, Stanford U., Phys. Dept. (2001).

[12] Patrick deNiverville, Maxim Pospelov, and Adam Ritz, “Observing a light dark matter beam with neutrino experiments,” Phys. Rev. **D84**, 075020 (2011), arXiv:1107.4580 [hep-ph].

[13] Yonatan Kahn, Gordan Krnjaic, Jesse Thaler, and Matthew Toups, “DAEDALUS and dark matter detection,” Phys. Rev. **D91**, 055006 (2015), arXiv:1411.1055 [hep-ph].

[14] Maxim Pospelov and Yu-Dai Tsai, “Light scalars and dark photons in Borexino and LSND experiments,” Phys. Lett. **B785**, 288–295 (2018), arXiv:1706.00424 [hep-ph].

[15] Gabriel Magill, Ryan Plestid, Maxim Pospelov, and Yu-Dai Tsai, “Dipole Portal to Heavy Neutral Leptons,” Phys. Rev. **D98**, 115015 (2018), arXiv:1803.03262 [hep-ph].

[16] Gabriel Magill, Ryan Plestid, Maxim Pospelov, and Yu-Dai Tsai, “Millicharged particles in neutrino experiments,” Phys. Rev. Lett. **122**, 071801 (2019), arXiv:1806.03310 [hep-ph].

[17] Carlos A. Argüelles, Matheus Hostert, and Yu-Dai Tsai, “Testing New Physics Explanations of MiniBooNE Anomaly at Neutrino Scattering Experiments,” Phys. Rev. Lett. **123**, 261801 (2019), arXiv:1812.08768 [hep-ph].

[18] Kevin J. Kelly and Yu-Dai Tsai, “Proton fixed-target scintillation experiment to search for millicharged dark matter,” Phys. Rev. **D100**, 015043 (2019), arXiv:1812.03998 [hep-ph].

[19] C. A. Argüelles *et al.*, “White Paper on New Opportuni-

ties at the Next-Generation Neutrino Experiments (Part 1: BSM Neutrino Physics and Dark Matter)," (2019), arXiv:1907.08311 [hep-ph].

[20] Yu-Dai Tsai, Patrick deNiverville, and Ming Xiong Liu, "The High-Energy Frontier of the Intensity Frontier: Closing the Dark Photon, Inelastic Dark Matter, and Muon g-2 Windows," (2019), arXiv:1908.07525 [hep-ph].

[21] Sacha Davidson, Steen Hannestad, and Georg Raffelt, "Updated bounds on millicharged particles," *JHEP* **05**, 003 (2000), arXiv:hep-ph/0001179 [hep-ph].

[22] Austin Ball *et al.*, "A Letter of Intent to Install a milli-charged Particle Detector at LHC P5," (2016), arXiv:1607.04669 [physics.ins-det].

[23] Andrew Haas, Christopher S. Hill, Eder Izaguirre, and Itay Yavin, "Looking for milli-charged particles with a new experiment at the LHC," *Phys. Lett.* **B746**, 117–120 (2015), arXiv:1410.6816 [hep-ph].

[24] Alexander Kusenko, Silvia Pascoli, and Dmitry Semikoz, "New bounds on MeV sterile neutrinos based on the accelerator and Super-Kamiokande results," *JHEP* **11**, 028 (2005), arXiv:hep-ph/0405198 [hep-ph].

[25] Peng-fei Yin and Shou-hua Zhu, "Detecting light long-lived particle produced by cosmic ray," *Phys. Lett.* **B685**, 128–133 (2010), arXiv:0911.3338 [hep-ph].

[26] Ping-Kai Hu, Alexander Kusenko, and Volodymyr Takhistov, "Dark Cosmic Rays," *Phys. Lett.* **B768**, 18–22 (2017), arXiv:1611.04599 [hep-ph].

[27] Torsten Bringmann and Maxim Pospelov, "Novel direct detection constraints on light dark matter," *Phys. Rev. Lett.* **122**, 171801 (2019), arXiv:1810.10543 [hep-ph].

[28] Carlos Argüelles, Pilar Coloma, Pilar Hernández, and Víctor Muñoz, "Searches for Atmospheric Long-Lived Particles," (2019), arXiv:1910.12839 [hep-ph].

[29] Pilar Coloma, Pilar Herández, Víctor Muñoz, and Ian M. Shoemaker, "New constraints on Heavy Neutral Leptons from Super-Kamiokande data," (2019), arXiv:1911.09129 [hep-ph].

[30] James Alvey, Miguel Campos, Malcolm Fairbairn, and Tevong You, "Light Dark Matter from Inelastic Cosmic Ray Collisions," *Phys. Rev. Lett.* **123**, 261802 (2020), [*Phys. Rev. Lett.* 123, 261802(2019)], arXiv:1905.05776 [hep-ph].

[31] C. M. G. Lattes, H. Muirhead, G. P. S. Occhialini, and C. F. Powell, "PROCESSES INVOLVING CHARGED MESONS," *International Conference to Celebrate the 40th Anniversary of the Pion (40 PI) Bristol, England, July 22-24, 1987*, *Nature* **159**, 694–697 (1947), [,42(1947)].

[32] S. H. Neddermeyer and C. D. Anderson, "Note on the Nature of Cosmic Ray Particles," *Phys. Rev.* **51**, 884–886 (1937).

[33] R. Abbasi *et al.* (IceCube), "The IceCube Data Acquisition System: Signal Capture, Digitization, and Timestamping," *Nucl. Instrum. Meth.* **A601**, 294–316 (2009), arXiv:0810.4930 [physics.ins-det].

[34] K. Abe *et al.*, "Calibration of the Super-Kamiokande Detector," *Nucl. Instrum. Meth.* **A737**, 253–272 (2014), arXiv:1307.0162 [physics.ins-det].

[35] K. Abe *et al.* (Hyper-Kamiokande), "Hyper-Kamiokande Design Report," (2018), arXiv:1805.04163 [physics.ins-det].

[36] Zelimir Djurcic *et al.* (JUNO), "JUNO Conceptual Design Report," (2015), arXiv:1508.07166 [physics.ins-det].

[37] B. Abi *et al.* (DUNE), "The DUNE Far Detector Interim Design Report Volume 1: Physics, Technology and Strategies," (2018), arXiv:1807.10334 [physics.ins-det].

[38] Leonid Chuzhoy and Edward W. Kolb, "Reopening the window on charged dark matter," *JCAP* **0907**, 014 (2009), arXiv:0809.0436 [astro-ph].

[39] David Dunsky, Lawrence J. Hall, and Keisuke Horigaya, "CHAMP Cosmic Rays," *JCAP* **1907**, 015 (2019), arXiv:1812.11116 [astro-ph.HE].

[40] P. F. Smith, "Searches for fractional electric charge in terrestrial materials," *NEW AND EXOTIC PHENOMENA. PROCEEDINGS, 7TH MORIOND WORKSHOP, LES ARCS, FRANCE, JANUARY 24-31, 1987*, *Ann. Rev. Nucl. Part. Sci.* **39**, 73–111 (1989), [,527(1987)].

[41] M. I. Dobroliubov and A. Yu. Ignatiev, "MILlicharged Particles," *Phys. Rev. Lett.* **65**, 679–682 (1990).

[42] E. Golowich and R. W. Robinett, "Limits on Millicharged Matter From Beam Dump Experiments," *Phys. Rev.* **D35**, 391 (1987).

[43] K. S. Babu, Thomas M. Gould, and I. Z. Rothstein, "Closing the windows on MeV Tau neutrinos," *Phys. Lett.* **B321**, 140–144 (1994), arXiv:hep-ph/9310349 [hep-ph].

[44] S. N. Gninenko, N. V. Krasnikov, and A. Rubbia, "Search for millicharged particles in reactor neutrino experiments: A Probe of the PVLAS anomaly," *Phys. Rev.* **D75**, 075014 (2007), arXiv:hep-ph/0612203 [hep-ph].

[45] Judd D. Bowman, Alan E. E. Rogers, Raul A. Monsalve, Thomas J. Mozdzen, and Nivedita Mahesh, "An absorption profile centred at 78 megahertz in the sky-averaged spectrum," *Nature* **555**, 67–70 (2018), arXiv:1810.05912 [astro-ph.CO].

[46] Julian B. Muñoz and Abraham Loeb, "A small amount of mini-charged dark matter could cool the baryons in the early Universe," *Nature* **557**, 684 (2018), arXiv:1802.10094 [astro-ph.CO].

[47] Rennan Barkana, Nadav Joseph Outmezguine, Diego Redigolo, and Tomer Volansky, "Signs of Dark Matter at 21-cm?" (2018), arXiv:1803.03091 [hep-ph].

[48] Hongwan Liu, Nadav Joseph Outmezguine, Diego Redigolo, and Tomer Volansky, "Reviving Millicharged Dark Matter for 21-cm Cosmology," *Phys. Rev.* **D100**, 123011 (2019), arXiv:1908.06986 [hep-ph].

[49] Bob Holdom, "Two U(1)'s and Epsilon Charge Shifts," *Phys. Lett.* **166B**, 196–198 (1986).

[50] Nima Arkani-Hamed, Douglas P. Finkbeiner, Tracy R. Slatyer, and Neal Weiner, "A Theory of Dark Matter," *Phys. Rev.* **D79**, 015014 (2009), arXiv:0810.0713 [hep-ph].

[51] Maxim Pospelov, "Secluded U(1) below the weak scale," *Phys. Rev.* **D80**, 095002 (2009), arXiv:0811.1030 [hep-ph].

[52] Prateek Agrawal, Francis-Yan Cyr-Racine, Lisa Randall, and Jakub Scholtz, "Make Dark Matter Charged Again," *JCAP* **1705**, 022 (2017), arXiv:1610.04611 [hep-ph].

[53] Noah Kurinsky, Daniel Baxter, Yonatan Kahn, and Gordan Krnjaic, "A Dark Matter Interpretation of Excesses in Multiple Direct Detection Experiments,"

(2020), arXiv:2002.06937 [hep-ph].

[54] Alan E. Robinson and Émile Michaud, “Comment on A dark matter interpretation of excesses in multiple direct detection experiments [arXiv:2002.06937],” (2020), arXiv:2002.08893 [hep-ph].

[55] K. Bays *et al.* (Super-Kamiokande), “Supernova Relic Neutrino Search at Super-Kamiokande,” Phys. Rev. **D85**, 052007 (2012), arXiv:1111.5031 [hep-ex].

[56] M. Ambrosio *et al.* (MACRO), “A Search for lightly ionizing particles with the MACRO detector,” Phys. Rev. **D62**, 052003 (2000), arXiv:hep-ex/0002029 [hep-ex].

[57] M. Ambrosio *et al.* (MACRO), “Final search for lightly ionizing particles with the MACRO detector,” (2004), arXiv:hep-ex/0402006 [hep-ex].

[58] S. I. Alvis *et al.* (Majorana), “First Limit on the Direct Detection of Lightly Ionizing Particles for Electric Charge as Low as $e/1000$ with the Majorana Demonstrator,” Phys. Rev. Lett. **120**, 211804 (2018), arXiv:1801.10145 [hep-ex].

[59] A. A. Aguilar-Arevalo *et al.* (MiniBooNE DM), “Dark Matter Search in Nucleon, Pion, and Electron Channels from a Proton Beam Dump with MiniBooNE,” (2018), arXiv:1807.06137 [hep-ex].

[60] R. Acciari *et al.* (ArgoNeuT), “Improved Limits on Millicharged Particles Using the ArgoNeuT Experiment at Fermilab,” (2019), arXiv:1911.07996 [hep-ex].

[61] Serguei Chatrchyan *et al.* (CMS), “Search for Fractionally Charged Particles in pp Collisions at $\sqrt{s} = 7$ TeV,” Phys. Rev. **D87**, 092008 (2013), arXiv:1210.2311 [hep-ex].

[62] Hendrik Vogel and Javier Redondo, “Dark Radiation constraints on minicharged particles in models with a hidden photon,” JCAP **1402**, 029 (2014), arXiv:1311.2600 [hep-ph].

[63] Joerg Jaeckel, Martin Jankowiak, and Michael Spannowsky, “LHC probes the hidden sector,” Phys. Dark Univ. **2**, 111–117 (2013), arXiv:1212.3620 [hep-ph].

[64] M. Mori *et al.* (Kamiokande-II), “Search for fractionally charged particles in Kamiokande-II,” Phys. Rev. **D43**, 2843–2846 (1991).

[65] M. Aglietta *et al.*, “Search for fractionally charged particles in the Mont Blanc LSD scintillation detector,” Astropart. Phys. **2**, 29–34 (1994).

[66] R. Agnese *et al.* (CDMS), “First Direct Limits on Lightly Ionizing Particles with Electric Charge Less Than $e/6$,” Phys. Rev. Lett. **114**, 111302 (2015), arXiv:1409.3270 [hep-ex].

[67] Haim Goldberg and Lawrence J. Hall, “A new candidate for dark matter,” Physics Letters B **174**, 151–155 (1986).

[68] Timon Emken, Rouven Essig, Chris Kouvaris, and Mukul Sholapurkar, “Direct Detection of Strongly Interacting Sub-GeV Dark Matter via Electron Recoils,” JCAP **1909**, 070 (2019), arXiv:1905.06348 [hep-ph].

[69] Roni Harnik, Zhen Liu, and Ornella Palamara, “Millicharged Particles in Liquid Argon Neutrino Experiments,” JHEP **07**, 170 (2019), arXiv:1902.03246 [hep-ph].

[70] Zuowei Liu, Yong-Heng Xu, and Yu Zhang, “Probing dark matter particles at CEPC,” JHEP **06**, 009 (2019), arXiv:1903.12114 [hep-ph].

[71] S. L. Dubovsky, D. S. Gorbunov, and G. I. Rubtsov, “Narrowing the window for millicharged particles by CMB anisotropy,” JETP Lett. **79**, 1–5 (2004), [Pisma Zh. Eksp. Teor. Fiz. 79, 3 (2004)], arXiv:hep-ph/0311189 [hep-ph].

[72] A. D. Dolgov, S. L. Dubovsky, G. I. Rubtsov, and I. I. Tkachev, “Constraints on millicharged particles from Planck data,” Phys. Rev. **D88**, 117701 (2013), arXiv:1310.2376 [hep-ph].

[73] Ely D. Kovetz, Vivian Poulin, Vera Gluscevic, Kimberly K. Boddy, Rennan Barkana, and Marc Kamionkowski, “Tighter limits on dark matter explanations of the anomalous EDGES 21 cm signal,” Phys. Rev. **D98**, 103529 (2018), arXiv:1807.11482 [astro-ph.CO].

[74] L. Singh *et al.* (TEXONO), “Constraints on millicharged particles with low threshold germanium detectors at Kuo-Sheng Reactor Neutrino Laboratory,” Phys. Rev. **D99**, 032009 (2019), arXiv:1808.02719 [hep-ph].

[75] S. N. Glinenko, D. V. Kirpichnikov, and N. V. Krasnikov, “Probing millicharged particles with NA64 experiment at CERN,” (2018), arXiv:1810.06856 [hep-ph].

[76] Jinhan Liang, Zuowei Liu, Yue Ma, and Yu Zhang, “Millicharged particles at electron colliders,” (2019), arXiv:1909.06847 [hep-ph].

[77] Paul A. M. Dirac, “Quantized Singularities in the Electromagnetic Field,” Proc. Roy. Soc. Lond. **A133**, 60–72 (1931), [278(1931)].

[78] Jogesh C. Pati and Abdus Salam, “Unified Lepton-Hadron Symmetry and a Gauge Theory of the Basic Interactions,” Phys. Rev. **D8**, 1240–1251 (1973).

[79] H. Georgi and S. L. Glashow, “Unity of All Elementary Particle Forces,” Phys. Rev. Lett. **32**, 438–441 (1974).

[80] Howard Georgi, “The State of the Art—Gauge Theories,” *PARTICLES AND FIELDS — 1974: Proceedings of the Williamsburg Meeting of APS/DPF*, AIP Conf. Proc. **23**, 575–582 (1975).

[81] Harald Fritzsch and Peter Minkowski, “Unified Interactions of Leptons and Hadrons,” Annals Phys. **93**, 193–266 (1975).

[82] Gary Shiu, Pablo Soler, and Fang Ye, “Milli-Charged Dark Matter in Quantum Gravity and String Theory,” Phys. Rev. Lett. **110**, 241304 (2013), arXiv:1302.5471 [hep-th].

[83] M. Tanabashi *et al.* (Particle Data Group), “Review of Particle Physics,” Phys. Rev. **D98**, 030001 (2018).

[84] Torsten Bringmann, Joakim Edsjö, Paolo Gondolo, Piero Ullio, and Lars Bergström, “DarkSUSY 6 : An Advanced Tool to Compute Dark Matter Properties Numerically,” JCAP **1807**, 033 (2018), arXiv:1802.03399 [hep-ph].

[85] M. J. Boschini *et al.*, “Solution of heliospheric propagation: unveiling the local interstellar spectra of cosmic ray species,” Astrophys. J. **840**, 115 (2017), arXiv:1704.06337 [astro-ph.HE].

[86] L. B. Auerbach *et al.* (LSND), “Measurement of electron - neutrino - electron elastic scattering,” Phys. Rev. **D63**, 112001 (2001), arXiv:hep-ex/0101039 [hep-ex].

[87] N. Abgrall *et al.* (LEGEND), “The Large Enriched Germanium Experiment for Neutrinoless Double Beta Decay (LEGEND),” *Proceedings, Matrix Elements for the Double beta decay Experiments (MEDEX'17): Prague, Czech Republic*, AIP Conf. Proc. **1894**, 020027 (2017), arXiv:1709.01980 [physics.ins-det].

[88] John F. Beacom and Mark R. Vagins, “GADZOOKS! Anti-neutrino spectroscopy with large water Cherenkov detectors,” Phys. Rev. Lett. **93**, 171101 (2004),

arXiv:hep-ph/0309300 [hep-ph].

[89] Klaes Møller, Anna M. Suliga, Irene Tamborra, and Peter B. Denton, “Measuring the supernova unknowns at the next-generation neutrino telescopes through the diffuse neutrino background,” *JCAP* **1805**, 066 (2018), arXiv:1804.03157 [astro-ph.HE].

[90] Guanying Zhu, Shirley Weishi Li, and John F. Beacom, “Developing the MeV potential of DUNE: Detailed considerations of muon-induced spallation and other backgrounds,” *Phys. Rev.* **C99**, 055810 (2019), arXiv:1811.07912 [hep-ph].

[91] Fengpeng An *et al.* (JUNO), “Neutrino Physics with JUNO,” *J. Phys.* **G43**, 030401 (2016), arXiv:1507.05613 [physics.ins-det].

[92] J. Rich, R. Rocchia, and M. Spiro, “A Search for Strongly Interacting Dark Matter,” *NEW AND EXOTIC PHENOMENA. PROCEEDINGS, 7TH MORIOND WORKSHOP, LES ARCS, FRANCE, JANUARY 24-31, 1987*, *Phys. Lett.* **B194**, 173 (1987), [,221(1987)].

[93] Adrienne L. Erickcek, Paul J. Steinhardt, Dan McCammon, and Patrick C. McGuire, “Constraints on the Interactions between Dark Matter and Baryons from the X-ray Quantum Calorimetry Experiment,” *Phys. Rev.* **D76**, 042007 (2007), arXiv:0704.0794 [astro-ph].

[94] M. Shafi Mahdawi and Glennys R. Farrar, “Constraints on Dark Matter with a moderately large and velocity-dependent DM-nucleon cross-section,” *JCAP* **1810**, 007 (2018), arXiv:1804.03073 [hep-ph].

[95] Mark W. Goodman and Edward Witten, “Detectability of Certain Dark Matter Candidates,” *Phys. Rev.* **D31**, 3059 (1985), [,325(1984)].

[96] Glenn D. Starkman, Andrew Gould, Rahim Es-mailzadeh, and Savas Dimopoulos, “Opening the Window on Strongly Interacting Dark Matter,” *Phys. Rev.* **D41**, 3594 (1990).

[97] David N. Spergel and Paul J. Steinhardt, “Observational evidence for selfinteracting cold dark matter,” *Phys. Rev. Lett.* **84**, 3760–3763 (2000), arXiv:astro-ph/9909386 [astro-ph].

[98] Daniel Green *et al.*, “Messengers from the Early Universe: Cosmic Neutrinos and Other Light Relics,” *Bull. Am. Astron. Soc.* **51**, 159 (2019), arXiv:1903.04763 [astro-ph.CO].

[99] Asher Berlin, Dan Hooper, Gordan Krnjaic, and Samuel D. McDermott, “Severely Constraining Dark Matter Interpretations of the 21-cm Anomaly,” (2018), arXiv:1803.02804 [hep-ph].

[100] Jung-Tsung Li and Tongyan Lin, “Dynamics of millicharged dark matter in supernova remnants,” (2020), arXiv:2002.04625 [astro-ph.CO].

[101] Robert D. Pisarski, T. L. Trueman, and Michel H. G. Tytgat, “How $\pi^0 \rightarrow \gamma\gamma$ changes with temperature,” *Phys. Rev.* **D56**, 7077–7088 (1997), arXiv:hep-ph/9702362 [hep-ph].

[102] J. Wess and B. Zumino, “Consequences of anomalous Ward identities,” *Phys. Lett.* **37B**, 95–97 (1971).

[103] G. Agakishiev *et al.* (NA4), “Inclusive dielectron spectra in p+p collisions at 3.5 GeV,” *Eur. Phys. J.* **A48**, 64 (2012), arXiv:1112.3607 [nucl-ex].

[104] M. Aguilar-Benitez *et al.*, “Inclusive particle production in 400-GeV/c p p interactions,” *Z. Phys.* **C50**, 405–426 (1991).

[105] G. Jancso *et al.*, “Evidence for Dominant Vector Meson Production in Inelastic Proton Proton Collisions at 53-GeV Center-of-Mass Energy,” *Nucl. Phys.* **B124**, 1–11 (1977).

[106] Pierrick Marie Hanlet, *Inclusive Measurements of the Eta Cross Section at 38.8 GEV and the Branching Ratio for Eta Meson Going to Positive Muon Negative Muon.*, Ph.D. thesis, UNIVERSITY OF VIRGINIA. (1995).

[107] A. Baldini, V. Flaminio, W. G. Moorhead, and Douglas R. O. Morrison, *Total Cross-Sections for Reactions of High Energy Particles (Including Elastic, Topological, Inclusive and Exclusive Reactions) / Totale Wirkungsquerschnitte für Reaktionen hochenergetischer Teilchen (einschließlich elastischer, topologischer, inklusive)*, edited by H. Schopper, Landolt-Boernstein - Group I Elementary Particles, Nuclei and Atoms, Vol. 12b (Springer, 1988).

[108] A. Sibirtsev, W. Cassing, and U. Mosel, “Heavy meson production in proton - nucleus reactions with empirical spectral functions,” *Z. Phys.* **A358**, 357–367 (1997), arXiv:nucl-th/9607047 [nucl-th].

[109] Daniel M. Kaplan (E789), “Charmonium production in Fermilab E789,” *Quarkonium physics. Proceedings, UIC Workshop, Chicago, USA, June 13–15, 1996*, *Int. J. Mod. Phys.* **A12**, 3827–3836 (1997), arXiv:hep-ex/9610003 [hep-ex].

[110] I. Abt *et al.* (HERA-B), “Measurement of the J/ψ production cross section in 920-GeV/c fixed-target proton-nucleus interactions,” *Phys. Lett.* **B638**, 407–414 (2006), arXiv:hep-ex/0512029 [hep-ex].

[111] R. Vogt, “ J/ψ production and suppression,” *Phys. Rept.* **310**, 197–260 (1999).

[112] T. Alexopoulos *et al.* (E-771), “Differential cross-sections of J/ψ and ψ -prime in 800-GeV/c p-Si interactions,” *Phys. Rev.* **D55**, 3927–3932 (1997).